White-light upconversion emission of lanthanide double-doped oxide nanoparticles *via* defect state luminescence of ZnO

Yuemei Li[1], Yongmei Li[2], Rui Wang[1*] and Yanling Xu[1]

ABSTRACT   The white upconversion luminescence (UCL) of upconversion nanoparticles (UCNPs) is mainly made up of the color red, green and blue. Interestingly, the white-light-emitting UCNPs can be obtained *via* a complex method of tridoping lanthanide ions such as Yb^{3+}, Er^{3+}, and Tm^{3+}. We herein report that an excellent white UCL can be obtained from Yb/Tm double-doped ZnO. In this system, the blue and red UCL-emissions around 475 and 652 nm originate from $^1G_4 \rightarrow {}^3H_6$ and $^1G_4 \rightarrow {}^3F_4$ transition of Tm^{3+}, respectively, and the green one can be attributed to the defect states (oxygen vacancies) luminescence (DSL) of the ZnO host. Meanwhile, the fine nanostructure of ZnO:Yb/Tm is prepared by adjusting the concentration of OH^-. Particularly, the one dimentional pencil-shaped nanorods with high aspect ratio achieve a strong green DSL emission due to the high concentration of oxygen vacancy. The oxygen vacancy defects play an irreplaceable role in affecting the intensities of blue and red UCL by acting as the intermediate state in the energy transfer process. More importantly, we demonstrate that the DSL and UCL can be combined into systems, paving a new road for obtaining the white UCL emission.

Keywords: white upconversion luminescence, pencil-shaped ZnO:Yb/Tm nanorods, defect states luminescence

INTRODUCTION

Recently, lanthanide (Ln^{3+}= Yb, Er, Tm, and Ho) codoped upconversion nanoparticles (UCNPs) have attracted significant attention due to their outstanding energy transfer (ET) properties. The doping of Ln^{3+} ions can convert the near-infrared (NIR) into visible light. The NIR excitation can penetrate the skin, which has potential biological applications, such as bioimaging and multi-functional biological probes [1–15]. The white UCL has a broad range of emission wavelengths, including blue, green, and red emissions, generating a large library of spectral region that can be used for multiplexed biological labeling and encoding [16,17]. However, the relatively low efficiency of white UCL sources still poses a challenge to researchers today. It is well-known that the efficiency of white UCL is highly dependent on host matrix, particle morphology, crystallite phase, and lanthanide dopants [18–23]. Therefore, the study of their host matrix is important for obtaining a good white UCL emission and white light [24].

Previous studies on host materials have been focused on various semiconductor nanocrystals such as Gd_2O_3 and ZnO [25,26]. A significant improvement in ET from the semiconductor nanocrystals (SNC) has led to an efficiently sensitized UCL emission. Meanwhile, the inefficient absorptions of the forbidden 4f-4f transitions of Ln ions have been overcome [27]. With the doped $(Eu^{3+})Y_2O_3$ nanocrystals, it was reported that the UCL intensity of SNC was enhanced *via* the ET from the excited host to the Eu^{3+} ions [28]. This phenomenon was explained by host sensitization, which occurred due to energy level fitting in the crystal field structure of Ln^{3+} ions in the SNC lattice sites [29]. ZnO SNCs are the most common host materials of a UCL system, owing to their electronic structures and optical properties. In particular, ZnO nanorods have attracted great interest due to their high surface-to-volume ratio and excellent crystallite quality [30,31]. However, it is difficult to incorporate Ln^{3+} ions into the ZnO lattice due to the large mismatch of ionic radii between Ln^{3+} and Zn^{2+} ions and the resulting imbalance in charge [32,33].

[1] School of Chemistry and Chemical Engineering, Harbin Institute of Technology, Harbin 150001, China
[2] Key Laboratory of Hormones and Development (Ministry of Health), Tianjin Key Laboratory of Metabolic Diseases, Tianjin Metabolic Diseases Hospital & Tianjin Institute of Endocrinology, Tianjin Medical University, Tianjin 300070, China
* Corresponding author (email: wangrui001@hit.edu.cn)
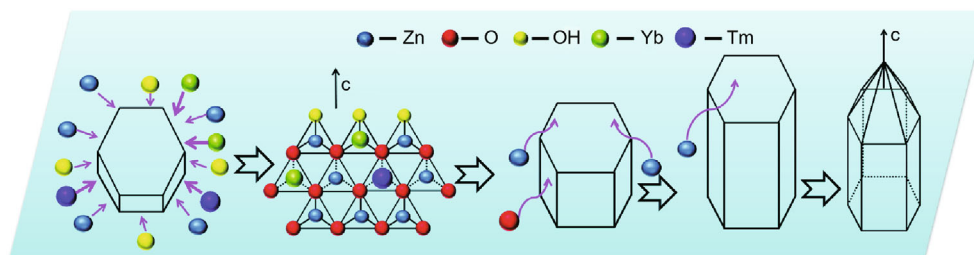
Scheme 1 Schematic illustration of the oriented growth mechanism of ZnO:Yb/Tm by controlling the concentration of OH⁻.

In this study, we proposed a hydrothermal wet chemical method to synthesize pencil-shaped ZnO:Yb/Tm nanorods, and demonstrated a novel strategy by which the defect states (oxygen vacancies) luminescence (DSL) of ZnO and intra-4f electronic transitions of Ln^{3+} were utilized to achieve the white UCL emission in a Yb^{3+} and Tm^{3+} co-doped ZnO SNC [34]. It is well-known that the efficiency of a white UCL depends on the concentrations of Ln^{3+} ions [35]. Here, for the first time, a white UCL is obtained through the double doping of Ln^{3+} ions into the ZnO SNCs. Specifically, the green UCL emission is obtained from the pencil-shaped ZnO by changing the concentrations of oxygen vacancies, and the cooperative emission of Yb^{3+}-Tm^{3+} provides the blue and red UCL emission.

EXPERIMENTAL SECTION

Synthesis
The hexagonal ZnO:Yb/Tm SNCs were synthesized *via* the hydrothermal method [30]. In our previous studies, we showed that the reaction time and temperature, the size of the samples, and the concentration of the doping ions affect the UCL properties of Yb/Tm/ZnO nanoparticles [30–36]. In order to analyze the functional dependence of the morphology, three sets of samples were prepared with different concentrations of OH⁻. While the molar concentrations of Yb^{3+} and Tm^{3+} were fixed at 7 and 0.5 mol% respectively, the OH⁻ concentrations were 1, 2 and 3 mol L^{-1} for the first, second, and third set, respectively [30]. A mixture of $Zn(NO_3)_2 \cdot 6H_2O$, $Yb(NO_3)_3 \cdot 5H_2O$ and $Tm(NO_3)_3 \cdot 5H_2O$ was dissolved by stirring for 1.5 h at 25°C. Then the solution was transferred to reaction kettle (30 mL) and reacted at 150°C for 24 h.

Characterization
The sample morphologies and sizes were analyzed by scanning electron microscopy (SEM; SU8000, Hitachi) and the transmission electron microscopy (TEM). The phase and structure of the sample were analyzed by X-ray diffraction (XRD) with a Rigaku Cu-Kα radiation (λ= 1.54 Å). The upconversion emission spectra of the Yb^{3+}/Tm^{3+}/ZnO nanoparticles were recorded using a 980 nm excitation. The color coordinates of the samples were calculated by the 1931 CIE (Commission Internationale de L'Eclairage France) system. All measurements were performed at room temperature.

RESULTS AND DISCUSSION

Structural characterization
As shown in Scheme 1, the size change and oriented growth of ZnO:Yb/Tm UCNPs can be controlled by the concentration of OH⁻. Fig. 1 shows the SEM and TEM images of the as-prepared ZnO: Yb/Tm (7/0.5 mol%) at different concentrations of sodium hydroxide (NaOH) from 1 to 3 mol L^{-1}. For the doping of 1 mol L^{-1} NaOH, the SEM and TEM images (Fig. 1a, d) show the ZnO:Yb/Tm UCNP composed of hexagonal microrods. When the concentration of NaOH was 2 mol L^{-1} (Fig. 1b, e), high-quality uniform pencil-shaped nanorods of ZnO:Yb/Tm UCNPs with pure hexagonal phase were achieved, and their sizes decreased from 210.4 to 96.3 nm (Fig. 1g). With 3 mol L^{-1} NaOH, the UCNPs show two dimensional (2D) structural growth such as dendrite and large-scale snowflake particles (Fig. 1c, f), and their sizes increase from 96.3 to 304.3 nm (Fig. 1g). Moreover, the energy dispersive X-ray spectrometry (EDS) analysis on pencil-shaped UCNPs shows the presence of Zn, Tm, and Yb elements only (Fig. 1h), proving no impurity. These results demonstrate that the size and oriented growth of ZnO:Yb/Tm UCNPs can be controlled by the doped OH⁻ contents. The growth process of ZnO:Yb/Tm includes the formation of $Zn(OH)_4^{2-}$, the dehydration of $Zn(OH)_4^{2-}$ at the crystal interface, and the substitution of lanthanide ions (Yb^{3+}/Tm^{3+}). The sample growth rate is related to the number of OH⁻ at the interface of ZnO_4^{6-}. The hydroxyl ion tends to stabilize the zinc ion and affects the direction
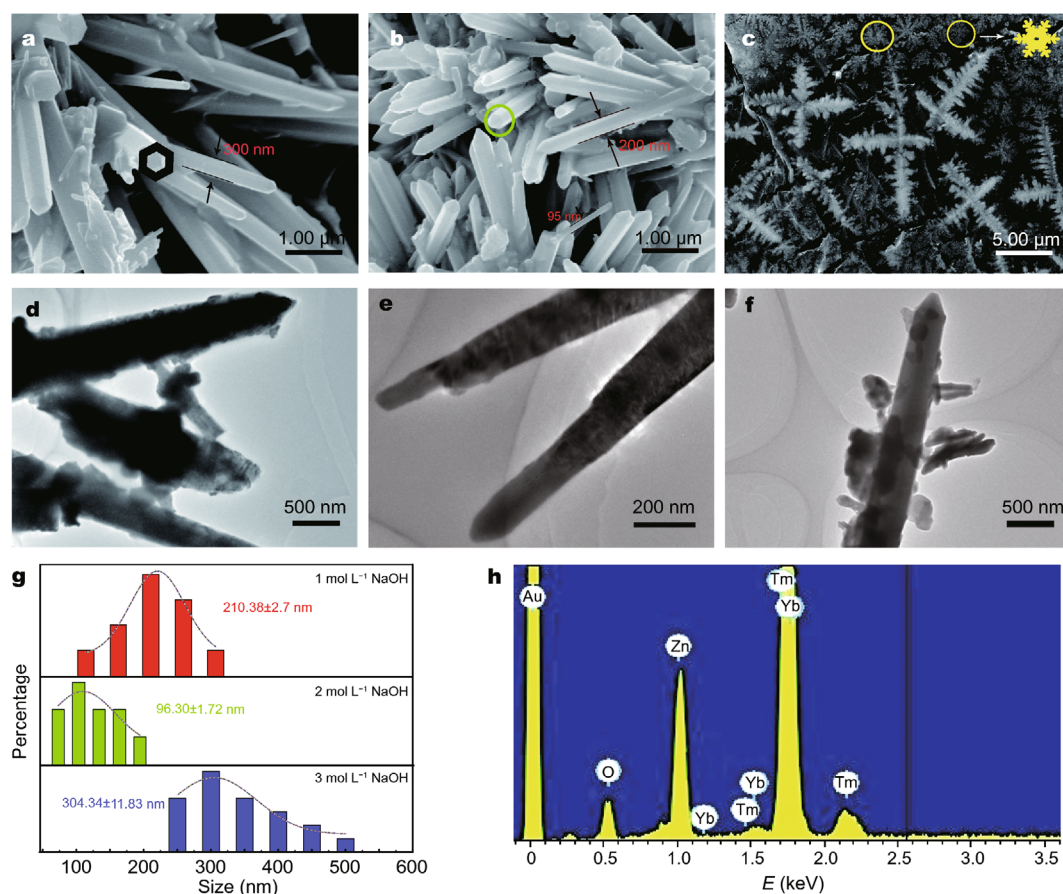
Figure 1 (a–c) Typical SEM images and (d–f) the TEM images of ZnO:Yb/Tm with OH⁻ contents of 1, 2 and 3 mol L⁻¹ respectively, (g) the diameter size of ZnO:Yb/Tm nanorods for increased OH⁻ contents, (h) EDS of the as-prepared samples shown in (b).

of crystal growth, resulting in a change in the morphology. At relatively low concentrations of OH⁻ (1 and 2 mol L⁻¹), the mobility of Zn^{2+} was sufficient and the diffusion length was enough to allow radial growth (Scheme 1). As the concentration of NaOH was increased, the zinc ion had low mobility because of the presence of more hydroxyl groups, which enabled the 2D growth of the sample. Therefore, the ZnO:Yb/Tm UCNPs exhibited a snowflake-like morphology (Fig. 1c, f).

According to the coordination polyhedron rule for growth habit of ZnO, the fastest growth rate is observed in the (0001) plane. Therefore, the growth of *c*-plane-(0001) nanorods (scheme 1) in our experiment is consistent with the theory. The TEM image of a single nanorod (Fig. 2b), taken from Fig. 2a, has a lattice spacing of 5.23 Å, matching well with the (002) crystal plane of the hexagonal phase (Fig. 2c), which belongs to the (0001) planes. Fig. 2c shows the XRD patterns of the as-prepared samples with different concentrations of NaOH. The XRD peaks are consistent with hexagonal wurtzite ZnO

(JCPDS Card No. 36-1451) and confirm the absence of any other impurity phase. Furthermore, the ZnO:Yb/Tm-(002) peak, which is directly related to the 1D growth of ZnO:Yb/Tm nanorods, shows a significant difference in the intensity with increasing OH⁻ concentration. These results show that the sample has a strong diffraction peak and a highly preferential orientation in the (002) crystallographic direction when the OH⁻ content reaches 2 mol L⁻¹. Therefore, the 1D growth of ZnO:Yb/Tm (pencil-shaped nanorods) can be controlled by changing the concentration of OH⁻.

White upconversion emission of ZnO:Yb/Tm
The white UCL emission has many potential applications in various fields such as biological labeling, imaging, and biological probes. However, it is still a great challenge to fine-tune the upconversion color output. In order to further demonstrate the white UCL properties of ZnO:Yb/Tm UCNPs with different NaOH concentrations, we performed experiments with a laser irradiation of
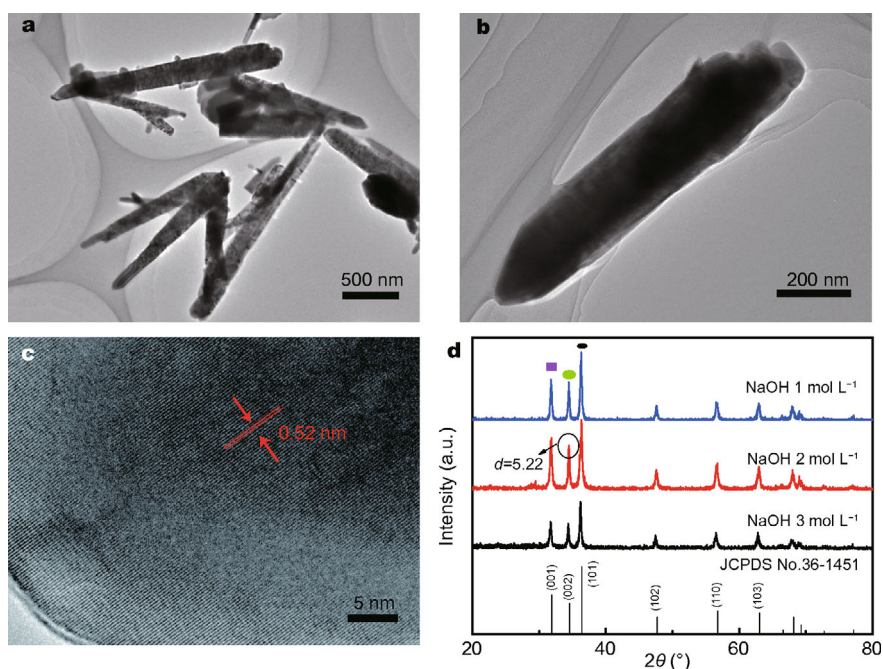
Figure 2 TEM images of ZnO:Yb/Tm nanorods with 2 mol L^{-1} of OH$^-$ with scale bar of 500 nm (a) and 200 nm (b), (c) high-resolution TEM image taken from a single particle in (b), (d) XRD patterns of the ZnO:Yb/Tm (7/0.5 mol%) by doping different OH$^-$ contents.
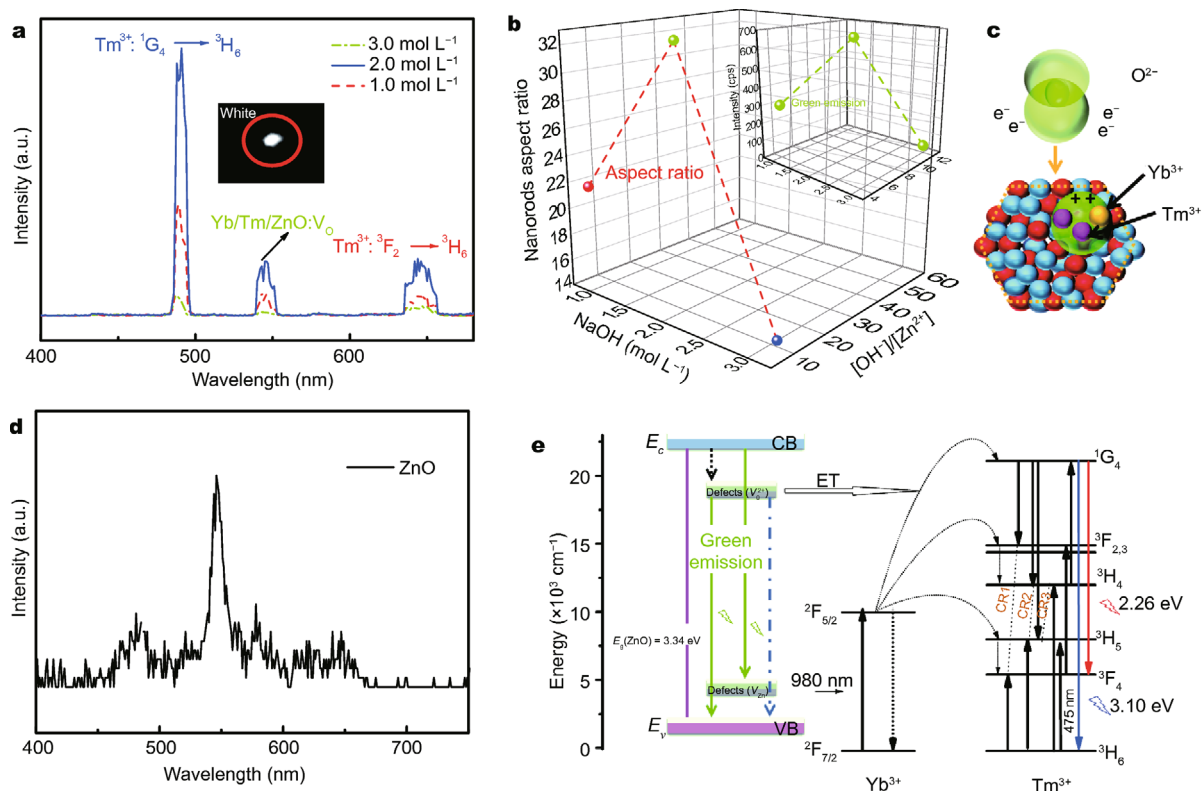

Figure 3 (a) UCL spectra of the samples with different content of OH$^-$, and the inset is a digital photograph; (b) the aspect ratio and intensity of green emission with different content of OH$^-$; (c) the change in surface charge density caused by replacing the Yb^{3+}/Tm^{3+} in the host lattice; (d) UCL spectra of the host ZnO with 2 mol L^{-1} of OH$^-$; (e) DSL and UCL mechanisms under the excitation of 980 nm laser.
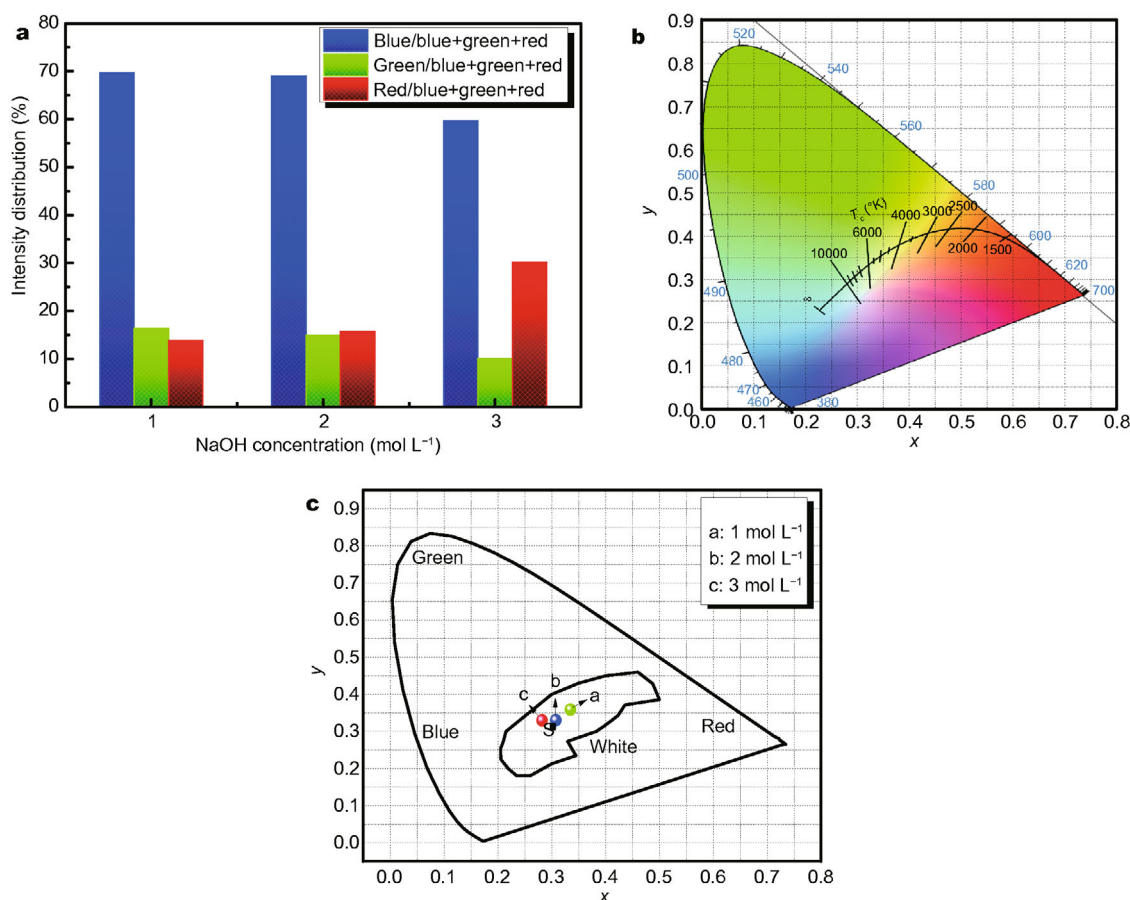
Figure 4 (a) $I_B/I_{(B+G+R)}$, $I_G/I_{(B+G+R)}$ and $I_R/I_{(B+G+R)}$ intensity distributions, (b, c) chromaticity diagram for the ZnO:Yb/Tm with different concentrations of OH⁻ under 980 nm excitation.

980 nm. Fig. 3a shows the upconversion spectra of ZnO: Yb/Tm UCNPs at different concentrations of NaOH. As can be seen, these samples emit blue, red, and green UCL around 475, 652, and 545 nm, respectively (Fig. 3a). The blue and red UCL originate from $^1G_4 \rightarrow {}^3H_6$ and $^1G_4 \rightarrow {}^3F_4$, respectively (Fig. 3e). On the other hand, the green UCL can be ascribed to the DSL. The UCL emission intensity of ZnO:Yb/Tm reaches a maximum with 2 mol L⁻¹ OH⁻, indicating an ET process from the host ZnO to Yb^{3+} and Tm^{3+}, while the defect states (oxygen vacancies) act as the intermediate states. In addition, the aspect ratio of nanorods and the intensity of green UCL peak at this OH⁻ concentration (Fig. 3b). This indicates that the high aspect ratio of pencil-shaped nanorods produces a high quantity of oxygen vacancies, which prefers the DSL process and a strong green UCL emission is consequently observed. Meanwhile, the substitutions of Zn^{2+} by Yb^{3+} and Tm^{3+} generate positive dipoles pointing outward on the crystal surface (to balance the charge), subsequently

attracting oxygen ions in the periphery, which can greatly accelerate the formation of oxygen vacancies from the solution to the grain, and therefore promote the intensity of green UCL emission (Fig. 3c). In order to further determine the source of the green UCL emission band centered around 545 nm under the excitation with 980 nm, the UCL emission spectra of the host ZnO nanoparticles were recorded. The corresponding spectrum (Fig. 3d) shows one emission band centered at 545 nm. Therefore, the band originates from the DSC of ZnO nanoparticles.

The digital photograph (inset of Fig. 3a) shows white color. In order to further investigate the white UCL intensity of ZnO:Yb/Tm with different OH⁻ concentrations, the color distributions of samples are analyzed. Fig. 4a shows the intensity distributions of $I_B/I_{(B+G+R)}$, $I_G/I_{(B+G+R)}$, and $I_R/I_{(B+G+R)}$ in the range from 400 to 750 nm, where B, G, and R represent the blue, green, and red emissions, respectively. It was found that the emission proportion of

$I_R/I_{(B+G+R)}$ increased, while $I_B/I_{(B+G+R)}$ and $I_G/I_{(B+G+R)}$ decreased gradually with increasing OH^- concentration. This result can be attributed to the morphology of the samples, because the formation of dendrite structures (see Fig. 1) increases as the concentration of OH^- increases. Moreover, to analyze the color composition of the white emissions that the naked eye perceives, the color coordinates were calculated from Fig. 3a *via* the 1931 CIE (Commission Internationale de I'Eclairage France) system. As illustrated in Fig. 4b, c, the white UCL can be obtained by increasing the concentration of OH^- from 1 to 3 mol L^{-1}, and the chromaticity coordinates (x, y) change systematically from (0.335, 0.360) to (0.282, 0.330). It is worth pointing out that when the OH^- concentration is 2 mol L^{-1}, the ideal white UCL is achieved for the first time in the ZnO:Yb/Tm nanoparticles with color coordinates of (0.308, 0.330), which is very close to the standard white-light chromaticity coordinates of (0.33, 0.33). Therefore, the OH^- concentration can not only control the 1D growth of nanorods, but also significantly enhances the green DSL emission, further affecting the white UCL output.

CONCLUSION

In summary, we presented a novel way of generating the white UCL *via* Yb/Tm double-doped ZnO SNCs. The oxygen vacancies of the host ZnO SNCs play an important role as defecting states to provide the green UCL emission, while the doping of Yb/Tm lanthanide ions provides the blue and red UCL emissions. Interestingly, the 1D growth of pencil-shaped nanorods results in larger aspect ratio in these UCNPs systems, and results in a significantly enhanced intensity of green DSL emission as compared with that from the 2D growth of UCNPs, thus providing a facile and effective approach to obtain an excellent white UCL emission. Moreover, the oxygen vacancy states of ZnO nanocrystals provide the energy for the transition of Ln^{3+} (Yb/Tm) ions. Depending on the intermediate level of the ET process, a strong white UCL emission is obtained for the first time due to the strong blue and red emission of the doped nanocrystals. Our work offers a new way to achieve the white UCL emission and broaden the range of UCNPs.

1   Liu Y, Tu D, Zhu H, *et al.* Lanthanide-doped luminescent nano-bioprobes: from fundamentals to biodetection. Nanoscale, 2013, 5: 1369–1384

2   Wilhelm S, Kaiser M, Würth C, *et al.* Water dispersible upconverting nanoparticles: effects of surface modification on their luminescence and colloidal stability. Nanoscale, 2015, 7: 1403–1410

3   Wang M, Abbineni G, Clevenger A, *et al.* Upconversion nanoparticles: synthesis, surface modification and biological applications. Nanomed-Nanotech Biol Med, 2011, 7: 710–729

4   Wang L, Yan R, Huo Z, *et al.* Fluorescence resonant energy transfer biosensor based on upconversion-luminescent nanoparticles. Angew Chem Int Ed, 2005, 44: 6054–6057

5   Chen Z, Chen H, Hu H, *et al.* Versatile synthesis strategy for carboxylic acid-functionalized upconverting nanophosphors as biological labels. J Am Chem Soc, 2008, 130: 3023–3029

6   Cui HH, Valdez JG, Steinkamp JA, *et al.* Fluorescence lifetime-based discrimination and quantification of cellular DNA and RNA with phase-sensitive flow cytometry. Cytometry, 2003, 52A: 46–55

7   Steemers FJ, Ferguson JA, Walt DR. Screening unlabeled DNA targets with randomly ordered fiber-optic gene arrays. Nat Biotechnol, 2000, 18: 91–94

8   Han M, Gao X, Su JZ, *et al.* Quantum-dot-tagged microbeads for multiplexed optical coding of biomolecules. Nat Biotechnol, 2001, 19: 631–635

9   Creran B, Yan B, Moyano DF, *et al.* Laser desorption ionization mass spectrometric imaging of mass barcoded gold nanoparticles for security applications. Chem Commun, 2012, 48: 4543–4545

10 Zhang F, Haushalter RC, Haushalter RW, *et al.* Rare-earth upconverting nanobarcodes for multiplexed biological detection. Small, 2011, 7: 1972–1976

11 Cen Y, Wu YM, Kong XJ, *et al.* Phospholipid-modified upconversion nanoprobe for ratiometric fluorescence detection and imaging of phospholipase d in cell lysate and in living cells. Anal Chem, 2014, 86: 7119–7127

12 Liu J, Cheng J, Zhang Y. Upconversion nanoparticle based LRET system for sensitive detection of MRSA DNA sequence. Biosens Bioelectron, 2013, 43: 252–256

13 Zhang Y, Tang Y, Liu X, *et al.* A highly sensitive upconverting phosphors-based off-on probe for the detection of glutathione. Sensors Actuators B-Chem, 2013, 185: 363–369

14 Yu M, Lin J, Wang Z, *et al.* Fabrication, patterning, and optical properties of nanocrystalline YVO_4:A (A=Eu^{3+}, Dy^{3+}, Sm^{3+}, Er^{3+}) phosphor films *via* sol-gel soft lithography. Chem Mater, 2002, 14: 2224–2231

15 Zhang F, Braun GB, Shi Y, *et al.* Fabrication of Ag@SiO_2@Y_2O_3:Er nanostructures for bioimaging: tuning of the upconversion fluorescence with silver nanoparticles. J Am Chem Soc, 2010, 132: 2850–2851

16 Zhang F, Wan Y, Yu T, *et al.* Uniform nanostructured arrays of sodium rare-earth fluorides for highly efficient multicolor upconversion luminescence. Angew Chem Int Ed, 2007, 46: 7976–7979

17 Liu Y, Tu D, Zhu H, *et al.* Lanthanide-doped luminescent nanoprobes: controlled synthesis, optical spectroscopy, and bioapplications. Chem Soc Rev, 2013, 42: 6924

18 Gorris HH, Wolfbeis OS. Photonen aufkonvertierende nanopartikel zur optischen codierung und zum multiplexing von zellen, biomolekülen und mikrosphären. Angew Chem, 2013, 125: 3668–3686

19 Shan J, Kong W, Wei R, *et al.* An investigation of the thermal sensitivity and stability of the β-NaYF$_4$:Yb,Er upconversion nanophosphors. J Appl Phys, 2010, 107: 054901–054901

20 Yu W, Xu W, Song H, *et al.* Temperature-dependent upconversion luminescence and dynamics of NaYF$_4$:Yb^{3+}/Er^{3+} nanocrystals: influence of particle size and crystalline phase. Dalton Trans, 2014,

43: 6139–6147

21 Li Z, Wang L, Wang Z, et al. Modification of NaYF$_4$:Yb,Er@SiO$_2$ nanoparticles with gold nanocrystals for tunable green-to-red up-conversion emissions. J Phys Chem C, 2011, 115: 3291–3296

22 Zhao J, Lu Z, Yin Y, et al. Upconversion luminescence with tunable lifetime in NaYF$_4$:Yb,Er nanocrystals: role of nanocrystal size. Nanoscale, 2013, 5: 944–952

23 Lu Y, Lu J, Zhao J, et al. On-the-fly decoding luminescence life-times in the microsecond region for lanthanide-encoded suspen-sion arrays. Nat Commun, 2014, 5: 3741

24 Mahalingam V, Naccache R, Vetrone F, et al. Preferential sup-pression of high-energy upconverted emissions of Tm^{3+} by Dy^{3+} ions in Tm^{3+}/Dy^{3+}/Yb^{3+}-doped LiYF$_4$ colloidal nanocrystals. Chem Commun, 2011, 47: 3481–3483

25 Yang X, Li Q, Liu Z, et al. Pressure-induced amorphization in Gd$_2$O$_3$/Er^{3+} nanorods. J Phys Chem C, 2013, 117: 8503–8508

26 Wang X, Kong X, Yu Y, et al. Effect of annealing on upconversion luminescence of ZnO:Er^{3+} nanocrystals and high thermal sensi-tivity. J Phys Chem C, 2007, 111: 15119–15124

27 Luo W, Liu Y, Chen X. Lanthanide-doped semiconductor nano-crystals: electronic structures and optical properties. Sci China Mater, 2015, 58: 819–850

28 Liu L, Chen X. Energy levels, fluorescence lifetime and Judd-Ofelt parameters of Eu^{3+} in Gd$_2$O$_3$ nanocrystals. Nanotechnology, 2007, 18: 255704

29 Fan F, Feng Y, Tang P, et al. Synthesis and gas sensing perfor-mance of dandelion-like ZnO with hierarchical porous structure. Ind Eng Chem Res, 2014, 53: 12737–12743

30 Li Y, Wang R, Xu Y, et al. Structural characterizations and up-conversion emission in Yb^{3+}/Tm^{3+}co-doped ZnO nanocrystals by tri-doping with Ga^{3+} ions. RSC Adv, 2016, 6: 111052–111059

31 Liu Y, Luo W, Li R, et al. Near-infrared luminescence of Nd^{3+} and Tm^{3+} ions doped ZnO nanocrystals. Opt Express, 2009, 17: 9748–9753

32 Zeng X, Yuan J, Wang Z, et al. Nanosheet-based microspheres of Eu^{3+}-doped ZnO with efficient energy transfer from ZnO to Eu^{3+} at room temperature. Adv Mater, 2007, 19: 4510–4514

33 Frindell KL, Bartl MH, Popitsch A, et al. Sensitized luminescence of trivalent europium by three-dimensionally arranged anatase nanocrystals in mesostructured titania thin films. Angew Chem Int Ed, 2002, 41: 959–962

34 Jayalakshmi G, Saravanan K, Balasubramanian T. Impact of thiol and amine functionalization on photoluminescence properties of ZnO films. J Lumin, 2013, 140: 21–25

35 Chen D, Wang Y, Zheng K, et al. Bright upconversion white light emission in transparent glass ceramic embedding Tm^{3+}/Er^{3+}/Yb^{3+}: β-YF3 nanocrystals. Appl Phys Lett, 2007, 91: 251903

36 Li Y, Li Y, Wang R, et al. Enhancing upconversion luminescence by annealing processes and the high-temperature sensing of ZnO: Yb/Tm nanoparticles. New J Chem, 2017, 41: 7116–7122

Author contributions   Li Y designed and engineered the samples, performed the experiments and data analysis, and wrote the paper. Li Y conceived the post-fabrication tuning of random modes, and wrote the paper. Wang R performed the data analysis, and wrote the paper. Xu Y contributed to the theoretical analysis. All authors contributed to the general discussion.

Conflict of interest   The authors declare that they have no conflict of interest.

Yuemei Li is a doctor of material chemistry at Harbin Institute of Technology. Her research is focused on the preparation of nanoparticles doped with rare earth ions, and their luminescence properties for application in biological probes and optical thermometry.

Rui Wang is a professor of chemistry. She has authored more than 50 peer review papers on topics of the growth of nanoparticles and single crystals, and the development of luminescent materials. Her current research interests include the application of upconverting luminescent materials in biological probes, and optical thermometry based on upconverting luminescent materials doped with rare earth ions.

实现基于缺陷能级稀土双掺氧化锌上转换发光

李月梅[1]，李永梅[2]，王锐[1*]，徐衍岭[1]

摘要 上转换白光由红色、绿色和蓝色组成，而上转换白光通常是通过复杂的三掺杂稀土离子如Yb^{3+}、Er^{3+}和Tm^{3+}实现的. 本文报道了一个新型材料，通过Yb^{3+}、Tm^{3+}双掺ZnO实现上转换白光输出. 体系获得475 nm ($^1G_4 \rightarrow {}^3H_6$)上转换蓝光和652 nm ($^1G_4 \rightarrow {}^3F_4$)上转换红光，上转换绿光发射源于ZnO基质材料缺陷(氧空位)发光. 此外，通过调节OH^-的浓度可以调控纳米材料形貌. 尤其是铅笔状结构纳米棒由于表面具有高浓度的氧空位，实现了上转换绿光辐射. 同时氧空位缺陷作为能量传递过程的中间态能级，提高了上转换蓝光以及上转换红光的发光强度. 我们的研究首次将缺陷发光机理和上转换发光机理相结合，为实现上转换白光输出开辟了新道路.